



Contents lists available at ScienceDirect

Journal of King Saud University – Science

journal homepage: [www.sciencedirect.com](http://www.sciencedirect.com)

# Cytotoxicity and apoptosis response of hexagonal zinc oxide nanorods against human hepatocellular liver carcinoma cell line

Javed Ahmad<sup>a,\*</sup>, Rizwan Wahab<sup>a</sup>, Mohd Javed Akhtar<sup>b</sup>, Maqsood Ahamed<sup>b</sup><sup>a</sup> Chair for DNA Research, Zoology Department, College of Sciences, King Saud University, Riyadh 11451, Saudi Arabia<sup>b</sup> King Abdullah Institute for Nanotechnology, King Saud University, Riyadh, 11451, Saudi Arabia

## ARTICLE INFO

### Article history:

Received 8 August 2021

Revised 14 September 2021

Accepted 13 October 2021

Available online 23 October 2021

### Keywords:

Zinc oxide nanorods

X-ray diffraction pattern

FTIR spectroscopy

Human cell line

ROS

RT-PCR

## ABSTRACT

Hexagonal zinc oxide nanorods (ZnO-NRs) were prepared via solution process using zinc nitrate hexahydrate ( $\text{Zn}(\text{NO}_3)_2 \cdot 6\text{H}_2\text{O}$ , 0.25 M), hexamethylenetetramine (HMT) and sodium hydroxide at low concentration ( $4 \times 10^{-3}$  M in 100 ml of distilled water) and refluxed at 100 °C for an hour. The HMT was used because its act as a template for the nucleation and growth of zinc oxide nanorods. The X-ray diffraction patterns (XRD) clearly reveal that the grown product is pure zinc oxide. The diameters and lengths of the synthesized nanorods lie between 200 and 250 nm and 2–3  $\mu\text{m}$  respectively as observed from the field emission scanning electron microscopy (FESEM). The chemical functional properties was analyzed by Fourier Transform infra-red (FTIR) spectroscopy. This study was designed to show the possible effect of ZnO-NRs in human liver cancer (HepG2) cells. It induces cytotoxicity via reactive oxygen species (ROS), mitochondrial membrane potential. For gene expression analysis, it induces apoptotic gene marker P53, Bax, caspase3, Bcl2 genes. Based on analysis and observations, it concludes that the ZnO-NRs were utilized for toxicity at dose dependent via ROS generation against human hepato cellular liver carcinoma cell line.

© 2021 The Authors. Published by Elsevier B.V. on behalf of King Saud University. This is an open access article under the CC BY-NC-ND license (<http://creativecommons.org/licenses/by-nc-nd/4.0/>).

## 1. Introduction

Investigation of the toxicity of nanomaterials (NMs) is increasing due to the large production and incorporation of these materials in many products. The increase of these consumer products causes NMs release and bioavailability in the environment. Zinc oxide (ZnO) NMs are widely used in the manufacture of anti-fouling paints as well as skincare products. ZnONMs have excellent ultraviolet (UV)-absorbing properties and transparency to visible light, making these NMs excellent sunscreen agents (Vijayakumar et al., 2016; Chen et al., 2007). Additionally, the biocidal activity of ZnO NMs gives high potential for the applications in products such as foods, packaging, cosmetics, medicines and healthcare formulations (Kumar et al., 2017). Zinc oxide nanorods (ZnO-NRs) show wurtzite crystal structure, which is formed due to

interpenetrating hexagonal closely packed sub-lattices consisting of one specific kind of an atom. Wurtzite structure of ZnO results in higher chemical and mechanical stability (Gojova et al., 2006).

The ZnO-NRs shows a band-gap of about 3.37 eV with 60 meV of binding energy. This material showed anticancer activity in the non-viable cell and bactericidal property as well, so in increased use of ZnO NMs as an anticancer and antibacterial agent as well as biomedical image contrasting agent (Pande et al., 2007). Therefore, due of increasing application of ZnO-NRs day by day the demand is also increased. Hence, owing to which different approaches have come for the easy and large scale synthesis of ZnO-NRs.

Nanotechnology has tremendous innovation over the last decades. ZnO, which possesses unique properties like optical, semi-conducting etc. ZnO used in biomedical applications, drug delivery, gene delivery, and biosensing of a wide array of molecules of interest. (Zhang et al., 2013). Although applications of ZnONMs in biomedical field are increasing, however, preparation of biocompatible of ZnO-NRs is still challenging (Riggio et al., 2010). ZnO-NRs also used as an adhesion-resistant inducing death in anchorage-dependent cells (Lee et al., 2008). ZnO-NPs showed cytotoxicity on multi-type of tumor cells A549, MCF-7, and EMT-6 (Dang et al., 2021). ZnO-NRs biocompatibility studies on LE cells showed

\* Corresponding author.

E-mail address: [javedahmad@ksu.edu.sa](mailto:javedahmad@ksu.edu.sa) (J. Ahmad).

Peer review under responsibility of King Saud University.



that ZnO-NRs could be a non-toxic NM for biological applications (Gopikrishnan et al., 2010; 2011). Toxicological assessment of ZnO-NRs with *green microalgae*, *D.subspicatus* and *Tetraselmis sp* effects of oxidative stress induction through CAT activity (Almeida et al., 2021). ZnO-NRs does not affect any mortality in zebrafish embryos but it exhibited cytotoxicity of cell-death by exposed to MCF-7 breast cancer cell lines (Ali et al., 2021). On the Immunosensing platform built on ZnO-NRs for finding cancer cell (B-lympho- blastoid cell line IM9) reveal strong near-band-edge (NBE) emission (Tamashevskia et al., 2019). Neuro-toxicity of ZnO-NMs shows comparatively lower toxicity but ZnO-NRs prompted developmental neurotoxicity that subsequently developed to PD-like symptoms at high doses (Jin et al., 2021). The cellular uptake of gold NPs in Human liver cancer HepG2 cells was measured, and the results monitored that the order nanospheres > nanorods > nano stars. A study by ZnO-NRs on human alveolar adenocarcinoma cells induced oxidative stress and apoptosis (Ahamed et al., 2011). In this connection, Gold NRs exposed by the A549 cells are localized in membranous vesicles with mitochondrial swelling were also observed. High Quantity of ROS production proposed that the oxidative stress will be the main reason causing cytotoxicity (Tang et al., 2015). Cellulose mesh, deposited with ZnO-NRs clusters demonstrated excellent antimicrobial activity for gram negative (*E. coli*, *Pseudomonas aeruginosa*) and gram positive (*Staphylococcus aureus*, *Bacillus cereus*, *Streptococcus thermophilis*) bacteria (Bhutia et al., 2018). ZnO-NRs decorated with graphene nanoplatelets have proven it a promising agent against *C. albicans* infections (Ficociello et al., 2018). ZnO-NR exposed to MCF7 cells exhibited a decrease in proliferation with the surge of apoptosis compared to HaCaT cells. (Zanni et al., 2016). Nanorod (ZnO-FA *in vitro* efficacy of DOX loaded ZnO-FA (ZnO-FA-DOX) has been evaluated against breast cancer cells MDA-MB231, (Mitra et al 2012) showed the potential of ZnO-NRs to induce complement stimulation and inflammatory response, changes in expression of genes involved in apoptosis and oxidative stress. (Aula et al., 2018).

The current study aimed to synthesize ZnO-NRs using zinc nitrate hexahydrate ( $Zn(NO_3)_2 \cdot 6H_2O$ ) and hexamethylenetetramine (HMT) via solution process and used as an anticancer material and also to assess the toxicity against Hepatocellular liver carcinoma cell lines (HepG2), testing cytotoxicity, intracellular ROS and apoptotic gene markers were discussed.

## 2. Materials and methods

### 2.1. Chemicals and reagents

The Zinc nitrate hexahydrate ( $Zn(NO_3)_2 \cdot 6H_2O$ ), hexamethylenetetramine (HMT) and Sodium Hydroxide (NaOH) were purchased for this experiment from Aldrich chemical corporation. Fetal bovine serum, penicillin-streptomycin and LTR (LysoTracker™ Red DND-99) were purchased from Invitrogen Co. USA. DMEM F-12, MTT [3-(4,5-dimethyl thiazol-2-yl)-2,5-diphenyl tetrazolium bromide], pyruvic acid, perchloric acid, DHE (dihydroethidium), DAR-1 (4,5-Diamino-N,N,N',N'-tetraethylrhodamine), JC-1 (5,5',6,6'-Tetrachloro -1,1', 3,3'-tetraethyl-imidacarbocyanine iodide), were obtained from Sigma-Aldrich (Sigma-Aldrich, MO, USA). Ultrapure water was used from a Milli-Q system. All other chemicals used were of reagent grade.

### 2.2. Formation of hexagonal zinc oxide shaped nanorods

The formation of nanopowder of ZnO-NRs were accomplished with using precursor material zinc nitrate hexahydrate ( $Zn(NO_3)_2 \cdot 6H_2O$ ), hexamethylenetetramine ( $CH_2)_6N_4$ ) (HMT) and sodium

hydroxide (NaOH) as per the previously described protocol with modification (Wahab et al., 2007a,b). In a typical synthesis, a small amount of zinc nitrate hexahydrate ( $Zn(NO_3)_2 \cdot 6H_2O$ , 0.25 M) was dissolved in 100 ml of distilled water, and to this mixture a small amount of HMT ( $4 \times 10^{-3}$  M) was dissolved. A colorless solution was obtained and at this point pH was reached to 6.6. To this solution NaOH (0.1 M) was added drop by drop and again pH was observed which reaches to 12.3. The entire solution was stirred for 30 min for the complete dissolution and thereafter refluxed in a three-necked refluxing pot at 100 °C for an hour (h) for complete precipitation. Once the refluxing time completed, a white aqueous powder was settled at the bottom of refluxing pot, the pot was kept for 24 h at room temperature and the solution was washed with methanol several times and dried and was examined further.

### 2.3. Characterizations of ZnO-NRs

The morphological characterizations were conducted with using scanning electron microscopy (SEM). To analyze SEM, processed powder was consistently sprayed on carbon tape and transfer it into a sputtering chamber for 2–3 s with platinum coating. Once the sputtering was completed the sample holder was removed and fixed it into SEM for morphological analysis. The crystallinity and crystal phases of obtained as grown powder was determined by using X-ray powder diffractometer (XRD)  $Cu_{K\alpha}$  radiation ( $\lambda = 1.54178 \text{ \AA}$ ) Bragg angle ranging from 20° to 65° with 6°/min scanning speed. Also the Fourier transform infrared (FTIR) spectroscopy was analyzed in the range of 400–4000  $cm^{-1}$ .

### 2.4. Cell culture

Human liver cancer (HepG2) cells (ATCC, US) were maintained in DMEM culture medium supplemented with 10% fetal bovine serum (FBS), 100 U/mL penicillin as an antibiotic, and 100  $\mu g/mL$  streptomycin at 37 °C in a humidified 5%  $CO_2$  incubator.

### 2.5. Cell viability assays

MTT (3-(4,5-dimethylthiazol-2-yl)-2,5-diphenyltetrazolium bromide) assay was carried out according to the previously described (Mosmann, 1983) protocol with some minor modifications. The cells were passaged every 3–4 days. Approximately 20,000 cells were seeded in a 96-well plate with a clean, flat base for 24 h at 37 °C with humidified environment. On the following day, cells were treated with ZnO-NRs at different concentrations. The control cells were employed as a reference with the same conditions. After the exposure period (24 h), the MTT assay was performed by measuring absorbance at 570 nm with a plate reader (Synergy HT). Cell viability is given in the percentage of control cells, assuming 100% cell viability in the control.

$$\% \text{ viability} = \frac{[(\text{total cells} - \text{viable cells}) / \text{total cells}] \times 100}{100}$$

### 2.6. Detection of intracellular ROS

Detection of intracellular reactive oxygen assay ( $O_2^{\cdot-}$  and  $H_2O_2$ ) under physiological conditions were determined by their probe Dihydroethidium (DHE). DHE is a freely permeable probe, which react with the ROS  $O_2^{\cdot-}$  produces red fluorescent product known as ethidium or 2-hydroxyethidium (Peshavariya et al., 2007). Although, ROS is the combined form of many reactive  $O_2^{\cdot-}$  molecules but  $O_2^{\cdot-}$  and  $H_2O_2$  are largely responsible for cellular injury and signaling pathways. Therefore,  $O_2^{\cdot-}$  and  $H_2O_2$ . Due to intercalation with the DHE-derived making enhanced the nucleus bright from the rest of the cytoplasm (Nauseef, 2014). An increase in red fluo-

rescence treated cells besides control cells suggest a more production of  $O^{2-}$  Cells. For the experiment DHE were labeled at a final concentration of 10  $\mu$ M and incubated for 40 min. Plates were washed carefully with HBSS two to three times and imaging was accompanied by using filter in a fluorescence microscope (Leica DMi8, Germany).

### 2.7. Mitochondrial membrane potentials

MMP were determined by HepG2 cells in control and treated was determined by JC-1 (5,5',6,6'-Tetrachloro-1,1',3,3'-tetraethyl benzimidazolylcarbocyanine iodide). In healthy cells with high mitochondrial membrane potential, JC-1 forms complexes known as J-aggregates with intense fluorescence (Smiley et al., 1991). On the other hand, in apoptotic cells with lower membrane potential, JC-1 remains in the monomeric. Cells were seeded at appropriate densities in plate reader. After the treatment, media was aspirated and labeled with 5  $\mu$ M JC-1 in HEPES buffered HBSS for

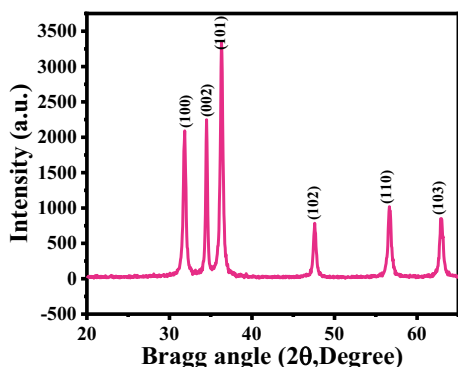


Fig. 1. X-ray diffraction pattern of grown ZnO-NRs via solution process.

20 min. Fluorescence of JC-1 aggregate (red in color) and JC-1 monomer (green in color) in cells were taken by a fluorescence microscope (Leica DMi8, using objective 20  $\times$  and LAS core software) using green filter cube.

### 2.8. Real-time PCR (RT-PCR)

Total RNA was purified from HepG2 cells from untreated and treated with ZnO-NRs for 24 h using the RNeasy mini Kit (Qiagen). As the manufacturing protocol RNA was isolated there purity were determined by Nanodrop 8000 spectrophotometer (Thermo Scientific, USA).

The integrity of RNA was confirmed by visualized on 2% agarose gel with the documentation system (Universal Hood II, BioRad, USA). The cDNA was prepared by the MLV reverse transcriptase (GE Health Care, UK) For the quantification of apoptotic of apoptotic and anti-apoptotic gene was determined by using Roche® LightCycler® 480 (96-well block), following the cycling program. Reaction mixture of 20  $\mu$ l taking 75 ng of the cDNA and 5  $\mu$ M of each primer with 2  $\times$  of SYBR Green I dye Roche Diagnostics. The cycling conditions at 95  $^{\circ}$ C for 10 min denaturation step, followed by 40 cycles of 95  $^{\circ}$ C for 15 s denaturation, 60  $^{\circ}$ C for 20 s annealing, and 72  $^{\circ}$ C for 20 s elongation steps. Data were normalized by GAPDH, a housekeeping control gene. All the experiment was done in triplicate.

### 2.9. Data analysis

ANOVA followed by Dunnett’s multiple comparison tests were used for statistical analysis data. Statistical significance was attributed at  $p < 0.05$ . Each experiment was carried in triplicates. Images were captured at constant exposure time

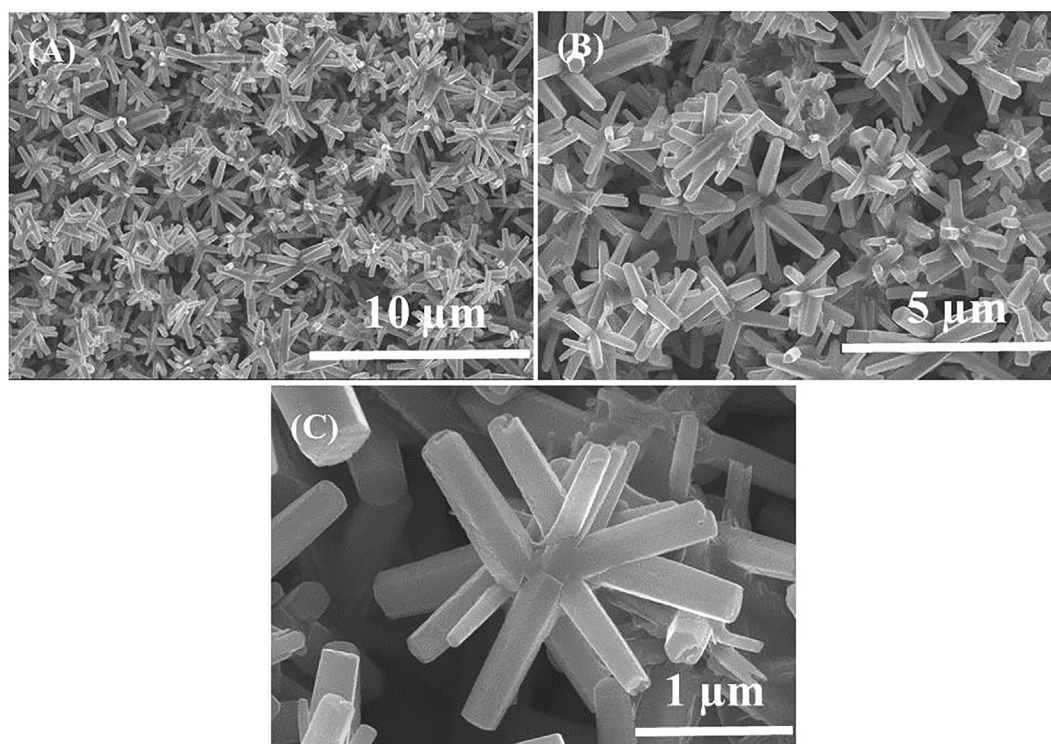


Fig. 2. Shows the FESEM images of flowers shaped morphology of ZnO-NRs: at low magnification (a and b) whereas (c) presents the high magnification.

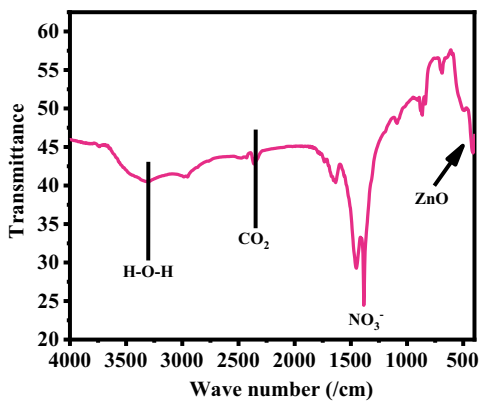


Fig. 3. FTIR Spectra of grown NRs.

### 3. Results

#### 3.1. X-ray diffraction (XRD) analysis

The XRD reveals the crystallite size, phases and crystallinity of the processed material. The assign peaks in the spectrum (Fig. 1) are well coordinated with a single crystalline wurtzite hexagonal phase bulk ZnO (JCPDS, Card No. 36-1451). No any other peaks or impurities again affirm that the processed material is well prepared and it's within the detection limit of the XRD. The sharp and strong intensity peaks in the diffraction spectrum displayed the good-crystallinity of synthesized powder.

#### 3.2. Morphological observations (FESEM result)

The morphology of the material was analyzed with FESEM and the data is represented as Fig. 2. From the obtained images, it reveals that the processed structure is full micro-flower shaped structures are seen with defied hexagonal nanorods. The average length and diameter of formed NRs are in the range of 2–4 μm (Fig. 2A and B), whereas the diameter of each NRs are varies form 200–250 nm. The individual NR surfaces are clear, smooth and hexagonal structure, which is a typical characteristic of wurtzite phase of zinc oxide (Fig. 2C). From the images it's evident that the entire rods shaped structures are originating from a center point and organize in such a way that they possess a spherical flower-like morphology. The NRs were jointed together through their wider bases in a spherical shape and form the flower-shaped structures. The full array of one flower-shaped structure is in the range of 2–3 μm.

#### 3.3. Functional groups analysis (FTIR spectroscopy results)

The functional characteristic of the processed powder was examined and assigned represent the FTIR spectroscopy as Fig. 3. The peak at 405 cm<sup>-1</sup> is related to zinc oxide whereas the bands at 3200–3600 cm<sup>-1</sup> correspond to O–H mode of vibration. The small asymmetric stretching mode of vibration of O–H was observed between 1629 cm<sup>-1</sup>. The symmetric and asymmetric stretching vibrational peak occurs between 1385 and 887 cm<sup>-1</sup> which designates the vibration of NO<sub>3</sub><sup>-1</sup> ions (Vijayakumar et al., 2016; Kumar et al., 2017).

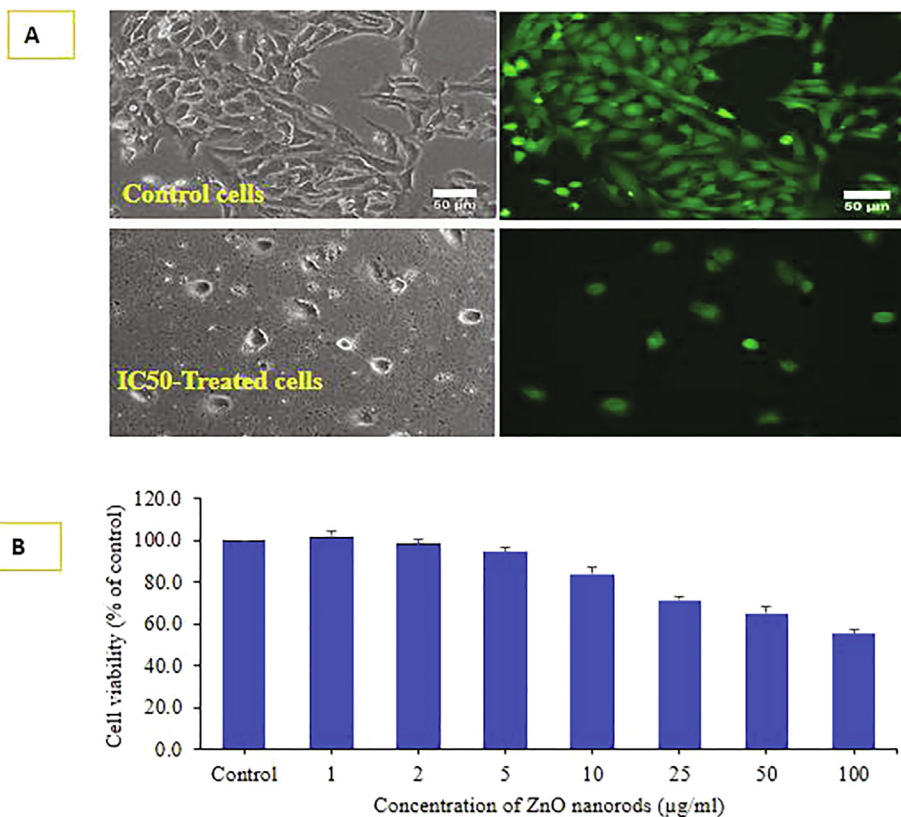


Fig. 4. Cell viability was determined by live cell imaging (A) due to treatment with IC50 of ZnONRs under phase contrast and calceinAM live cell fluorescent probe. Phase and calceinAM images represent superimposable pairs in control and treated groups. Cell viability was also determined by MTT assay is given in figure (B).Data represented are mean ± SD of three identical experiments in triplicates.

### 3.4. Cytotoxicity (MTT Assay) with ZnO-NRs

Cytotoxicity induction by ZnO-NRs in a concentration-dependent manner (Fig. 4A and B). Image of cell death morphology was taken only one concentration IC<sub>50</sub> and control HepG2 cells for 24 h treatment. The cancer cells HepG2 for MTT assay as with different concentrations of material from 2 to 100 µg/ml for 24 h incubation. It shows that viability of HepG2 cells was diminished by ZnO-NRs was concentration dependent. The cancer cells viability, with MTT assay was decreased at 24 h 101.7%, 98.3 %, 94.4%, 84%, 71.3%, 65% and 55% (Fig. 4B) for the concentrations range of 1, 2, 5, 10, 25 50 and 100 µg/mL respectively (p < 0.05 for each). It showed from the obtained data at high concentration is more affected.

### 3.5. ROS generation with ZnO-NRs induced HepG2 cells

ROS generation was examined in HepG2 cells after the exposure of ZnO-NRs at a concentration of 10, 25, 50, and 100 µg/ml for 24 h (Fig. 5A) with compared to control. As it can be observed from the image that the concentration of IC<sub>50</sub> and control (Fig. 5A) that ROS is increases with the increase of ZnO-NRs as compared to control cells. The ROS were upsurge at 10, 25, 50 and 100 µg/ml were 110, 138, 165, 185 % as compared to control (100%) (Fig. 5B). Data represented are mean ± SD of three identical experiments in triplicates. \*statistically significant difference as compared to the controls (p < 0.05).

### 3.6. Mitochondrial membrane potential (MMP) analysis induced ZnO-NRs

Degree of MMP induction was determined by the JC-1 imaging and JC-1 ratio of monomer/ aggregate both IC<sub>50</sub> and control HepG2 cells treated with ZnO-NRs (Fig. 6A). MMP level of percent control was determined at different concentration of ZnO-NRs in HepG2 cells exposed to for 24 h at 10, 25, 50 and 100 µg/ml are presented in Fig. 6B. The decrease in MMP level was recorded in terms of fluorescence intensity of mitochondrial-specific dye JC-1. It is clearly presented that ZnO-NRs decreased the fluorescence intensity.

### 3.7. Real time PCR induced by ZnO-NRs

For the gene expression analysis mRNA level was determined by quantitative RT-PCR with HepG2 cells treated ZnO-NRs for 24 h at a concentration of 100 µg/ml. Quantitative RT-PCR was performed to calculate the change of genes at the mRNA level (bax, p53, casp3, and bcl-2). The level of gene expression apoptotic gene fold changes for bax 1.8, p53 2.2 casp3 2.9 and anti-apoptotic gene bcl2 showed 0.6 fold respectively (Fig. 7). Data represented are mean ± SD of three identical experiments in triplicates. \*statistically significant difference as compared to the controls (p < 0.05).

### 3.8. Discussion

Based on the experimental and their observations related to work, we have discussed here that the hexagonal shaped ZnO

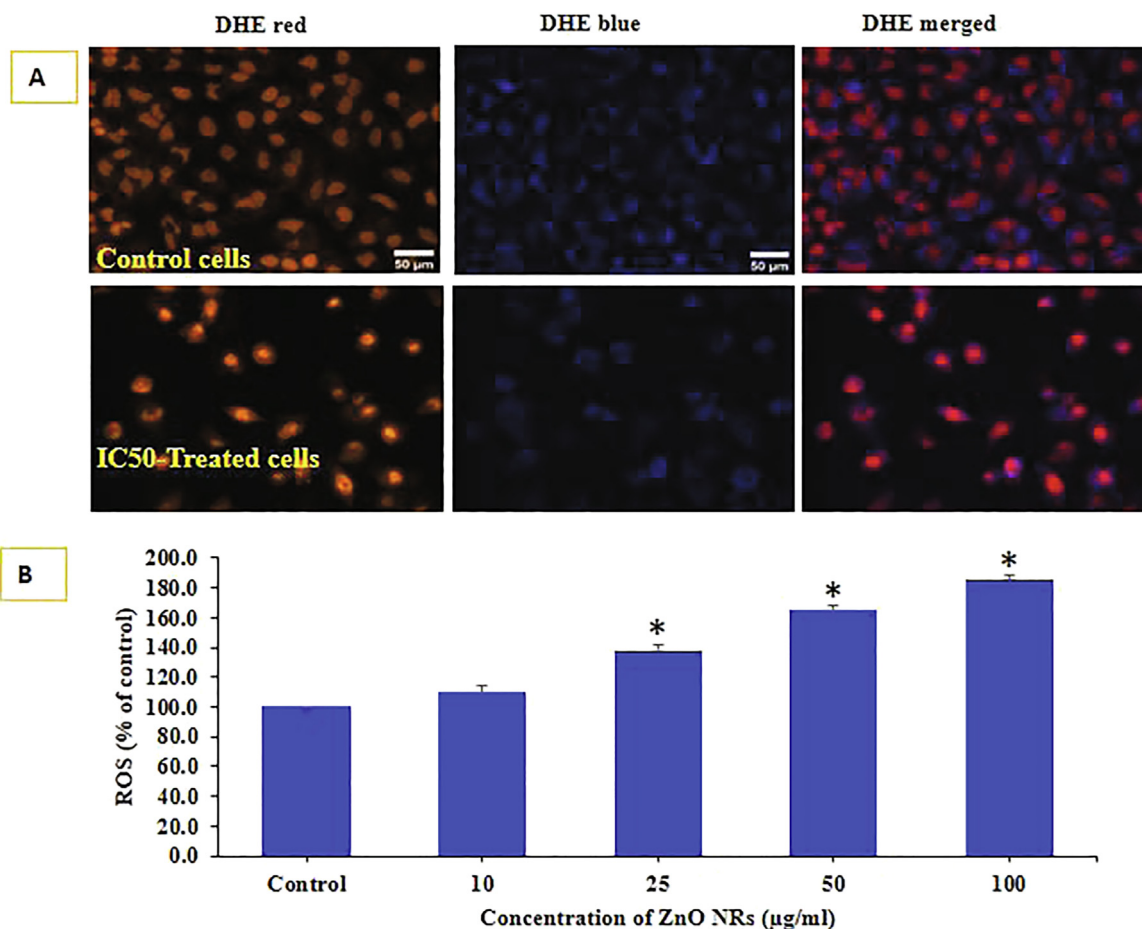
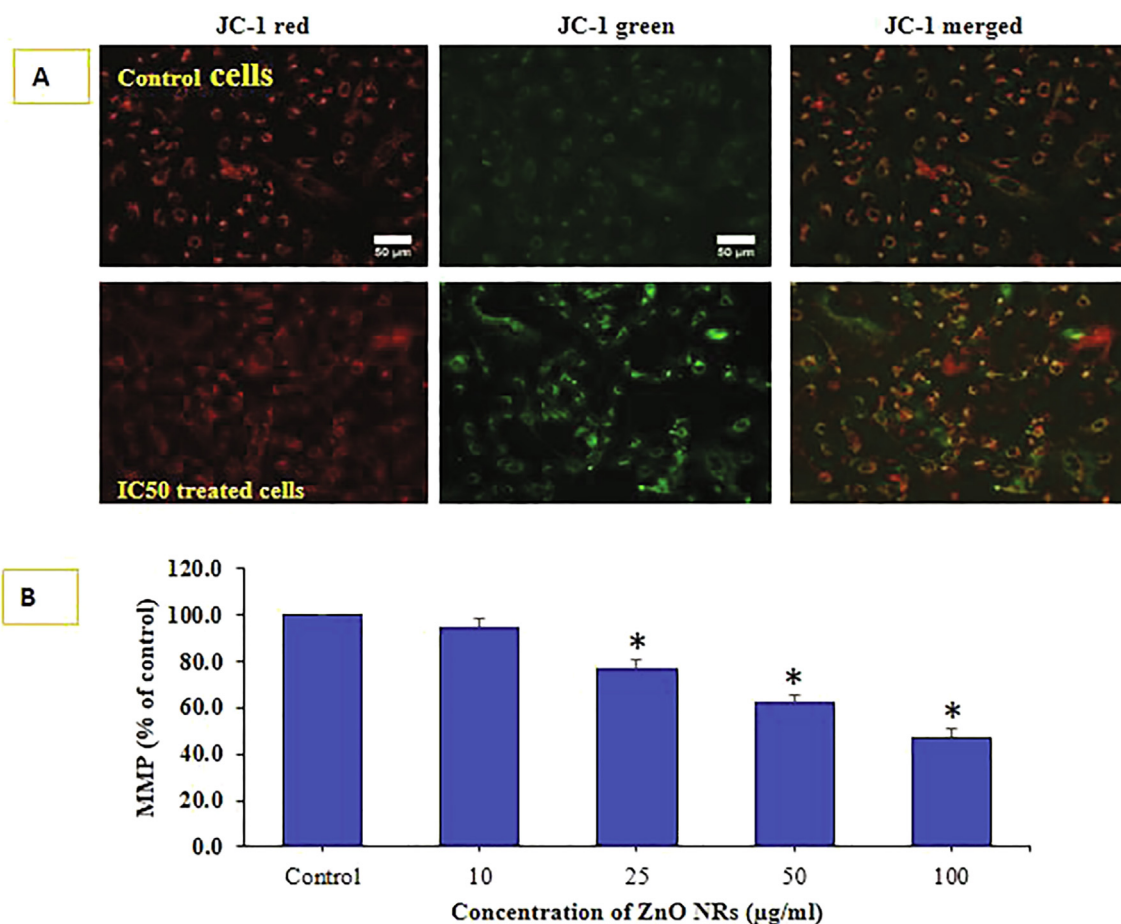
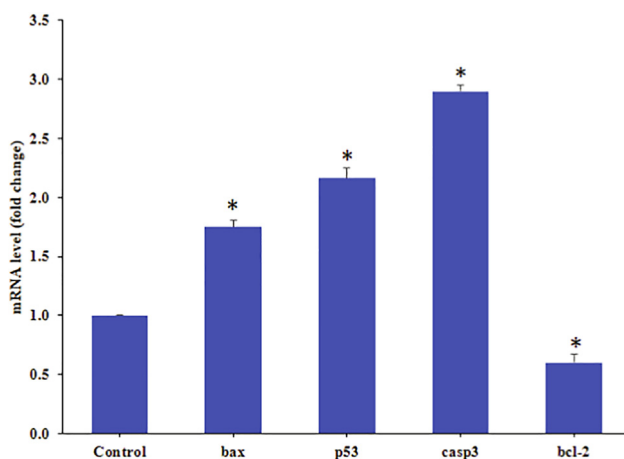


Fig. 5. ROS was detected by DHE probe in control and IC<sub>0</sub>-treated NPs in HepG2 cells in Fig. 5 (A). Live cell images were taken in tandem for DHE red and DHE blue. Quantification of DHE red fluorescence calculated in Image J software (NIH,US) is given in Fig. 5. (B). Data represented are mean ± SD of three identical experiments in triplicates. \*statistically significant difference as compared to the controls (p < 0.05).



**Fig. 6.** MMP was detected by JC-1 in control and treated cells. Images taken in tandem for JC-1 aggregate (red) and JC-1 monomer (green) and merged Fig. 6 A. MMP level of percent control was determined at different concentration of ZnONRs Fig. 6 B. Data represented are mean ± SD of three identical experiments (n = 3) made in triplicates. \*statistically significant difference as compared to the controls (p < 0.05).



**Fig. 7.** Quantification of mRNA fold change, apoptotic genes (p53, bax, and casp3) and anti-apoptotic gene (bcl-2) was evaluated. HepG2 cells treated 50 µg/mL of ZnO-NRs for 24 h. For internal control GAPDH was used. The values are mean ± SE of three independent experiments. \*Statistically significant difference as compared to control (p < 0.05).

and a transparent solution was formed. We have used HMT to this solution because it acts as a structure directing agent. In this solution the NaOH was added as a wise in the beaker, at this point a small flocculent was seen in the beaker for few seconds and then it was disappeared. As we may assume that these initial flocculent is an initial molecule for the formation of hexagonal shaped zinc nanorods. It's evident that the solution method provides the bulk amount of nanorods shaped powder. The obtained liquidly product was eroded completely and dried for the purpose of biological study (Wahab et al., 2011). A number of reports published on the nanoparticles and related structures whereas a limited study is available on hexagonal shaped zinc oxide nanorods (Wahab et al., 2009). As we know that the inorganic based oxide nano or microstructures structures cytotoxicity depends on different chemical and physicochemical parameters (eg: size, shape, chemical compound, concentration, cells medium concentration, incubation periods etc) (Wahab et al., 2009). In the current case hexagonal shaped NRs, which exhibit a unique shaped structure with diameter about 200 nm and length varies to 2–3 µm, initially attach to the surface of the cancer cells. The cells provide spaces because the cells size (20 µm) is more as compared to the NRs facilitates to enter in to cells cytoplasm and react with the cells organelles and are responsible for cell death. It's also postulated that the reactive oxygen species (ROS), which is a key factor in cell death produces in cells interaction with the foreign materials, and are responsible to form the free radicals in cells. These free radicals

nanorods were prepared with HMT, zinc nitrate hexahydrate (Zn (NO<sub>3</sub>)<sub>2</sub>·6H<sub>2</sub>O) and alkali sodium hydroxide (NaOH). As detailed in the material and methods Zn(NO<sub>3</sub>)<sub>2</sub>·6H<sub>2</sub>O was dissolved in water

in cells reacted with the cells organelles and produce the enzymatic change, which are responsible for a deformation of the cells and their contents (Wahab et al., 2014, Dwivedi et al., 2014). The observed data MTT, MMP are well corroborated with the available results. The microscopic image proves that the cells viability effect with zinc oxide nanostructures. A number of studies are required to conclude the phenomena why these rods shaped structures are responsible for the cell death in cancer cells (Henderson et al., 2007).

#### 4. Conclusion

The summary of the present work demonstrates that, we have successfully fabricated the hexagonal shaped ZnO-NRs via solution process and well characterized. The XRD pattern reveals the processed nanorods crystalline property, size with size of nanostructures, in spite of this the morphology was also evaluated via FESEM and it demonstrates that each individual size of nanorod is ~ 250 nm in diameter and 2–3  $\mu\text{m}$  length with good crystalline in nature. The chemical functional characteristics of the processed material property analyzed through FTIR spectroscopy and it reveals that the material is pure zinc oxide with good chemical property. The MTT assay was utilized to check the viability of cells at dose dependent manner, which express that initial concentration is very important for the cells reduction. The result obtained in MMP level in HepG2 cells further reveals the significance of utilized nanostructures. The apoptosis in cells with NRs were also studied in presence of P53, Bax casapse 3, and Bcl2 and their experimental results showed that the ZnO-NRs exposed with apoptotic genes, which displayed the up-regulation activity while anti apoptotic gene (Bcl2) showed down-regulation activity in cancer cells. Based on the acquired data's and their observations related to the interaction of NRs and cancer cells are also explained. The utilized analysis and their observations, reveals that the ZnO-NRs are responsible for the cells death for ROS generation. The oxide based nanostructures opens a new phenomenon to use as a nanocarrier available at low cost and can be easily use in future.

#### Declaration of Competing Interest

The authors declare that they have no known competing financial interests or personal relationships that could have appeared to influence the work reported in this paper.

#### Acknowledgement

The authors are grateful to the Deanship of Scientific Research, King Saud University for funding through Vice Deanship of Scientific Research Chairs.

#### References

- Almeida, A.C.O., Santos, L.F., Vicentini, D.S., Matias, W.G., Melegari, S.P., 2021. Evaluation of toxicity of zinc oxide nanorods on green microalgae of freshwater and marine ecosystems. *Environ. Chem. Ecotoxicol.* 3, 85–90.
- Ali, S., Sudha, K.G., Karunakaran, G., Kowsalya, M., Kolesnikov, E., Rajeshkumar, M.P., 2021. Green synthesis of stable antioxidant, anticancer and photocatalytic activity of zinc oxide nanorods from *Lea asiatica* leaf. *J. Biotechnol.* 329, 65–79.
- Ahamed, M., Akhtar, M.J., Raja, M., Ahmad, I., Siddiqui, M.K.J., AlSalhi, M.S., Alrokayan, S.A., 2011. ZnO nanorod-induced apoptosis in human alveolar adenocarcinoma cells via p53, survivin and bax/bcl-2 pathways: role of oxidative stress. *Nanomed. Nanotechnol. Biol. Med.* 7 (6), 904–913.
- Aula, S., Lakkireddy, S., Kapley, A., Adimadhyam, V.N., Sharma, R.K., Uppin, S.G., Jamil, K., 2018. Route of administration induced in vivo effects and toxicity responses of Zinc Oxide nanorods at molecular and genetic levels. *Int. J. Nano Dimens.* 9 (2), 158–169.

- Bhutiya, P.L., Mahajan, M.S., Abdul Rasheed, M., Pandey, M., Zaheer Hasan, S., Misra, N., 2018. Zinc oxide nanorod clusters deposited seaweed cellulose sheet for antimicrobial activity. *Int. J. Biol. Macromol.* 112, 1264–1271.
- Chen, Z., Meng, H., Yuan, H., Xing, G., Chen, C., Zhao, F., Wang, Y., Zhang, C., Zhao, Y., 2007. Identification of target organs of copper nanoparticles with ICP-MS technique. *J. Radioanal. Nucl. Chem.* 272 (3), 599–603.
- Dang, Z., Sun, J., Fan, J., Li, J., Li, X., Chen, T., 2021. Zinc oxide spiky nanoparticles: A promising nanomaterial for killing tumor cells. *Mater. Sci. Eng., C* 124, 112071. <https://doi.org/10.1016/j.msec.2021.112071>.
- Dwivedi, S., Wahab, R., Khan, F., Mishra, Y.K., Musarrat, J., Al-Khedhairi, A.A., Al-Ahmad, A., 2014. Reactive oxygen species mediated bacterial biofilm inhibition via zinc oxide nano particles and their statistical determination. *PLoS ONE* 9 (11), e111289. <https://doi.org/10.1371/journal.pone.0111289>.
- Ficociello, G., De Caris, M., Trillò, G., Cavallini, D., Sarto, M., Uccelletti, D., Mancini, P., 2018. Anti-candidal activity and in vitro cytotoxicity assessment of graphene nanoplatelets decorated with zinc oxide nanorods. *Nanomaterials.* 8 (10), 752. <https://doi.org/10.3390/nano8100752>.
- Gopikrishnan, R., Zhang, K., Ravichandran, P., Biradar, S., Ramesh, V., Goornavar, V., Jeffers, R.B., Pradhan, A., Hall, J.C., Baluchamy, S., Ramesh, G.T., 2011. Epitaxial growth of the zinc oxide nanorods, their characterization and in vitro biocompatibility studies. *J. Mater. Sci.: Mater. Med.* 22 (10), 2301–2309.
- Gopikrishnan, R., Zhang, K., Ravichandran, P., Baluchamy, S., Ramesh, V., Biradar, S., Ramesh, P., Pradhan, J., Hall, J.C., Pradhan, A.K., Ramesh, G.T., 2010. Synthesis, characterization and biocompatibility studies of zinc oxide (ZnO) nanorods for biomedical application. *Nano-Micro Lett.* 2 (1), 31–36.
- Gojova, A., Guo, B., Kota, R.S., Rutledge, J.C., Kennedy, I.M., Barakat, A.I., 2006. Induction of inflammation in vascular endothelial cells by metal oxide nanoparticles effect of particle composition. *Environ. Health Perspect.* 115 (3), 403–409.
- Henderson, K.L., Belden, J.B., Coats, J.R., 2007. Mass balance of metolachlor in a grassed phytoremediation system. *Environ. Sci. Technol.* 41 (11), 4084–4089.
- Jin, M., Li, N., Sheng, W., Ji, X., Liang, X., Kong, B., Yin, P., Li, Y., Zhang, X., Liu, K., 2021. Toxicity of different zinc oxide nanomaterials and dose-dependent onset and development of Parkinson's disease-like symptoms induced by zinc oxide nanorods. *Environ. Int.* 146, 106–179.
- Kumar, R., Umar, A., Kumar, G., Nalwa, H.S., 2017. Antimicrobial properties of ZnO nanomaterials: a review. *Ceram. Int.* 43 (5), 3940–3961.
- Lee, J., Kang, B.S., Hicks, B., Chancellor Jr., T.F., Chu, B.H., Wang, H.-T., Keselowsky, B. G., Ren, F., Lele, T.P., 2008. The control of cell adhesion and viability by zinc oxide nanorods. *Biomaterials* 29 (27), 3743–3749.
- Mitra, S., B., S., Patra, P., Chandra, S., Debnath, N., Das, S., Banerjee, R., Kundu, S.C., Pramanik, P., Goswami, A., 2012. Porous ZnO nanorod for targeted delivery of doxorubicin: in vitro and in vivo response for therapeutic applications. *J. Mater. Chem.* 22 (45), 24145. <https://doi.org/10.1039/c2jm35013k>.
- Mosmann, T., 1983. Rapid colorimetric assay for cellular growth and survival: application to proliferation and cytotoxicity assays. *J. Immunol. Methods.* 65 (1–2), 55–63.
- Nauseef, W.M., 2014. Detection of superoxide anion and hydrogen peroxide production by cellular NADPH oxidases. *Biochim. Biophys. Acta Gen. Subj.* 1840 (2), 757–767.
- Pande, P.C., Tiwari, L., Pande, H.C., 2007. Ethnoveterinary plants of Uttaranchal a review. *Indian J. Tradit. Know.* 6, 444–458.
- Peshavariya, H.M., Dusing, G.J., Selemidis, S., 2007. Analysis of dihydroethidium fluorescence for the detection of intracellular and extracellular superoxide produced by NADPH oxidase. *Free Radic. Res.* 41 (6), 699–712.
- Riggio, C., Raffa, V., Cuschieri, A., 2010. Synthesis, characterisation and dispersion of zinc oxide nanorods for biomedical applications. *Micro & Nano Lett.* 5 (5), 355–360.
- Smiley, S.T., Reers, M., Mottola-Hartshorn, C., Lin, M., Chen, A., Smith, T.W., Steele, G. D., Chen, L.B., 1991. Intracellular heterogeneity in mitochondrial membrane potentials revealed by a J-aggregate-forming lipophilic cation JC-1. *Proc. Natl. Acad. Sci.* 88 (9), 3671–3675.
- Tang, Y., Shen, Y., Huang, L., Lv, G., Lei, C., Fan, X., Lin, F., Zhang, Y., Wu, L., Yang, Y., 2015. In vitro cytotoxicity of gold nanorods in A549 cells. *Environ. Toxicol. Pharmacol.* 39 (2), 871–878.
- Tamashevski, A., Harmaza, Y., Viter, R., Jevdokimovs, D., Poplauskas, R., Slobozhanina, E., Mikoliunaite, L., Erts, D., Ramanaviciene, A., Ramanavicius, A., 2019. Zinc oxide nanorod based immunosensing platform for the determination of human leukemic cells. *Talanta* 200, 378–386.
- Vijayakumar, S., Vaseeharan, B., Malaikozhundan, B., Shobiya, M., 2016. Laurus nobilis leaf extract mediated green synthesis of ZnO nanoparticles: characterization and biomedical applications. *Biomed. Pharmacother.* 84, 1213–1222.
- Wahab, R., Ansari, S.G., Kim, Y.S., Seo, H.K., Kim, G.S., Khang, G., Shin, H.-S., 2007a. Low temperature solution synthesis and characterization of ZnO nano-flowers. *Mater. Res. Bull.* 42 (9), 1640–1648.
- Wahab, R., Ansari, S.G., Kim, Y.S., Seo, H.K., Kim, G.S., Khang, G., Shin, H.S., 2007b. Room temperature synthesis of needle-shaped ZnO nanorods via sonochemical method. *Appl. Surf. Sci.* 253 (18), 7622–7627.
- Wahab, R., Hwang, I.H., Kim, Y.-S., Shin, H.-S., 2011. Photocatalytic activity of zinc oxide micro-flowers synthesized via solution method. *Chem. Engg. J.* 168 (1), 359–366.
- Wahab, R., Kim, Y.-S., Hwang, I.H., Shin, H.-S., 2009. A non-aqueous synthesis, characterization of zinc oxide nanoparticles and their interaction with DNA. *Synth. Metals.* 159 (23–24), 2443–2452.

Wahab, R., Siddiqui, M.A., Saquib, Q., Dwivedi, S., Ahmad, J., Musarrat, J., Al-Khedhairy, A.A., Shin, H.-S., 2014. ZnO nanoparticles induced oxidative stress and apoptosis in HepG2 and MCF-7 cancer cells and their antibacterial activity. *Colloids Surf., B* 117, 267–276.

Zhang, Y., Nayak, T.R., Hong, H., Cai, W., 2013. Biomedical Applications of Zinc Oxide Nanomaterials. *Curr Mol Med.* 13 (10), 1633–1645.

Zanni, E., De Palma, S., Chandraiahgari, C.R., De Bellis, G., Cialfi, S., Talora, C., Palleschi, C., Sarto, M.S., Uccelletti, D., Mancini, P., 2016. In vitro toxicity studies of zinc oxide nano- and microrods on mammalian cells: A comparative analysis". *Mater. Lett.* 179, 90–94.